

# Charge-Density Wave in Overdoped Cuprates Driven by Electron-Phonon Couplings

Jiarui Liu,<sup>1</sup> Shaozhi Li,<sup>1</sup> Edwin Huang,<sup>2,3</sup> and Yao Wang<sup>1,4,\*</sup>

<sup>1</sup>*Department of Physics and Astronomy, Clemson University, Clemson, SC 29631, United States*

<sup>2</sup>*Department of Physics and Astronomy, University of Notre Dame, Notre Dame, IN 46556, United States*

<sup>3</sup>*Stavropoulos Center for Complex Quantum Matter,*

*University of Notre Dame, Notre Dame, IN 46556, United States*

<sup>4</sup>*Department of Chemistry, Emory University, Atlanta, GA 30322, United States*

(Dated: September 26, 2023)

Recent resonant x-ray scattering (RXS) experiments revealed a novel charge order in highly overdoped  $\text{La}_{2-x}\text{Sr}_x\text{CuO}_4$  (LSCO) [1]. The observed charge order appears around the  $(\pi/3, 0)$  wavevector and remains robust from cryogenic temperatures to room temperature. To investigate the origin of this charge order in the overdoped region, we use determinant quantum Monte Carlo (DQMC) simulations to examine models with various interactions. We demonstrate that this CDW originates from remnant correlations in overdoped cuprates. The doping-independent wavevector  $(\pi/3, 0)$  further reflects the presence of nonlocal electron-phonon couplings. Our study reveals the importance of phonons in the cuprates, which assist correlated electrons in the formation of exotic phases.

Unconventional superconductivity (SC) in cuprates has attracted extensive experimental and theoretical studies [2–6]. In addition to its promising applications in energy and quantum technology, the exploration of cuprates has been driven by numerous complex phases of cuprates [7]. These phases can coexist or compete with SC and have proven challenging to address within traditional solid-state frameworks. One prominent phase among these is the charge density wave (CDW). In conventional BCS superconductors, phonons mediate an effective electron-electron attraction that gives rise to both mobile Cooper pairs and immobile charge modulations. These two states compete against each other as evidenced by investigations into Holstein-like models [8–10]. In cuprates, despite having distinct pairing symmetry and likely different pairing mechanisms from BCS theory, many experiments have unveiled the presence of CDW orders or fluctuations near the SC phase. Their proximity suggests an intertwined origin of CDW and high- $T_c$  SC [11–15]. Furthermore, recent observations of CDW in infinite-layer nickelates [16–19] provide an additional example for the relation between these two states in unconventional superconductors analogous to cuprates.

Previous studies about CDW have been focused on underdoped and optimally doped cuprates [20–22], drawing significant attention to the intricate interplay between SC, pseudogap, and CDW [23–25]. Particularly, near 12.5% hole doping, charge order has been detected with a unidirectional stripe behavior and a periodicity of 4 unit cells [see Fig. 1]. Advanced numerical many-body methods have successfully captured and described this stripe order in the context of the Hubbard model [26, 27]. Remarkably, the CDW appearing in these simulations around 12.5% hole doping exhibits a notable competition with  $d$ -wave superconductivity [28–30].

Recently, CDWs in overdoped cuprates have been observed in BSCCO [31], prompting a novel exploration of their role in high- $T_c$  cuprates. This CDW phe-

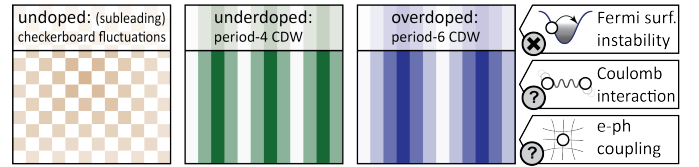


FIG. 1. Schematic illustrating different types of charge fluctuations or order observed from experiments across various doping regimes of cuprates. The origin of the overdoped period-6 CDW serves as the primary focus of this work.

nomenon was subsequently observed in extremely overdoped LSCO, in the form of a charge modulation of over 6 unit cells in the antinodal direction [see Fig. 1] and persists to room temperature [1]. (Here, we refer to the  $(H, 0)$  and  $(H, H)$  directions as “antinodal” and “nodal”, respectively) This CDW order starts to develop at 35% doping and maximizes its intensity at approximately 50% doping. Despite the expected screening of Coulomb interactions in the overdoped regime, Fermi-surface instabilities cannot explain the origin of this CDW [1]. Consequently, it is likely driven by interactions. Residing away from the SC and pseudogap phases, the overdoped regime may experience less influence from the dominant spin fluctuations, providing a unique opportunity to reveal intrinsic yet subleading interactions in cuprates.

For this purpose, we examine the extremely overdoped cuprates using various correlated models, including the Hubbard model, the Hubbard-Holstein model, and their variants. Our findings reveal that while the Hubbard interaction correctly produces a correlation-induced charge instability maximized at 50% doping, it fails to capture the charge pattern with wavevector  $(\pi/3, 0)$ . The inclusion of electron-phonon coupling (EPC), particularly nonlocal EPC, shifts the ordering wavevector from  $(\pi, \pi)$  towards the anticipated  $(\pi/3, 0)$ . Building upon this framework, we quantify the strength and distribution of the EPC, addressing the experimental observations in

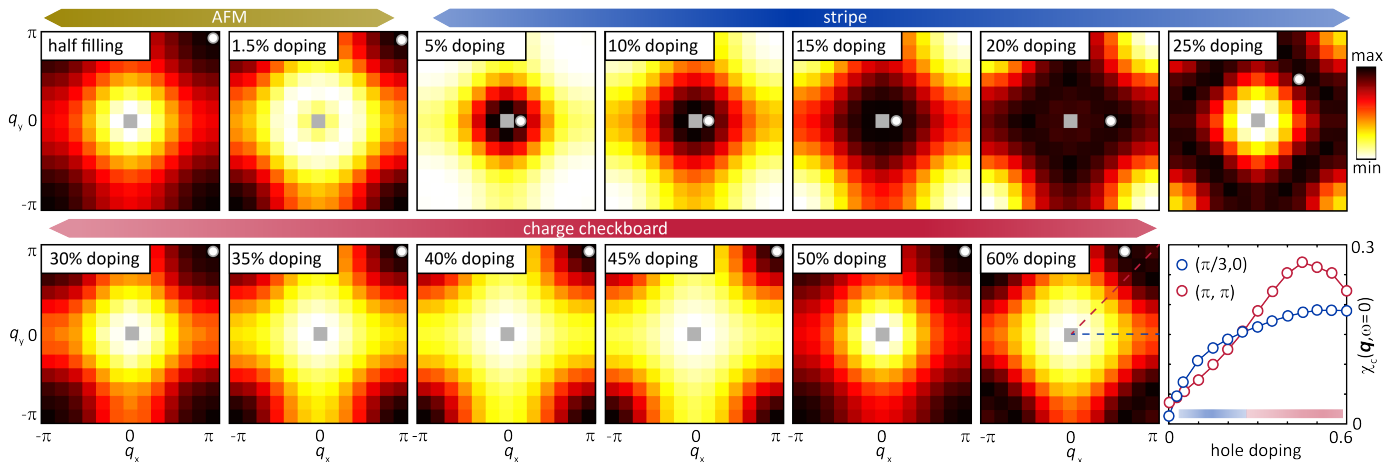


FIG. 2. The charge susceptibility  $\chi_c(\mathbf{q}, \omega = 0)$  obtained from the Hubbard model on a  $12 \times 12$  square lattice at temperature  $T = 0.4t$ . The susceptibility is normalized for each doping (panel). The white circles mark the maximal instability among all momenta for each doping. The upper ribbons indicate the corresponding phase. The last panel summarizes the doping dependence of charge susceptibility at  $\mathbf{q} = (\pi, \pi)$  and  $(\pi/3, 0)$  [experimentally relevant momentum].

LSCO. This work underscores the essential contributions of EPC to correlated phases in cuprates.

To capture the correlations, our theoretical study starts from the single-band Hubbard model [32, 33]:

$$\mathcal{H}_{\text{Hubbard}} = - \sum_{ij\sigma} t_{ij} c_{i\sigma}^\dagger c_{j\sigma} - \mu \sum_{i\sigma} n_{i\sigma} + \sum_i U n_{i\uparrow} n_{i\downarrow},$$

where  $c_{i\sigma}$  ( $c_{i\sigma}^\dagger$ ) annihilates (creates) an electron at site  $i$  with spin  $\sigma$  and  $n_{i\sigma} = c_{i\sigma}^\dagger c_{i\sigma}$  is the density operator. The hopping term is governed by the one-electron integral  $t_{ij}$  of Wannier wavefunctions at site  $i$  and  $j$ . With tight-binding assumption, we constrain the hopping to the nearest and next-nearest neighbors (denoted as  $t$  and  $t'$ , respectively). The Coulomb interaction is simplified to the on-site Hubbard interaction  $U$  and the chemical potential  $\mu$  determines the electron filling within the grand canonical ensemble. To reflect the electronic structure in LSCO, we use  $t' = -0.15t$  and  $U = 8t$  throughout the main text [34, 35], while the  $t'$  dependence is discussed in the Supplementary Material (SM) [36].

We employ the determinant quantum Monte Carlo (DQMC) algorithm to simulate the Hubbard model, considering that the overdoped CDW is persistent at high temperatures [1, 31]. DQMC is an unbiased quantum many-body method, which maps the thermal density matrix into a summation over Hubbard–Stratonovich field configurations that is estimated stochastically through importance sampling [37, 38]. This work aims to address the charge order in the RXS experiments and primarily focuses on the charge susceptibility  $\chi_c(\mathbf{q}, \omega)$  at  $\omega = 0$

$$\chi_c(\mathbf{q}, \omega = 0) = \int_0^\beta d\tau \sum_{i,j} e^{-i\mathbf{q}\cdot(\mathbf{r}_i - \mathbf{r}_j)} \times (\langle n_i(\tau) n_j(0) \rangle - \langle n_i(\tau) \rangle \langle n_j(0) \rangle). \quad (1)$$

Here,  $\beta = 1/T$  is the inverse temperature and  $n_i = n_{i,\uparrow} + n_{i,\downarrow}$ . If interactions are neglected,  $\chi_c$  can be evaluated using the Lindhard response function, which fails to explain the observed CDW as discussed in Ref. 1.

With the Hubbard model, we examine the impact of strong electron-electron correlations on overdoped cuprates. Figure 2 shows the doping dependence and momentum dependence of  $\chi_c$  at  $T = 0.4t$ . We employ a  $12 \times 12$  square cluster to preserve the  $D_{4h}$  symmetry, which is necessary for an unbiased comparison of charge instabilities along the nodal and antinodal directions. Since the overall charge susceptibility varies from almost zero at half-filling to substantial values at large dopings, in our figures, we normalize  $\chi_c(\mathbf{q}, \omega)$  at each doping by its maximal intensity to reflect the relative distribution of spectral weight in momentum space.

As the doping increases, the Hubbard model exhibits three discernible charge fluctuation behaviors. At and near half filling, the dominant antiferromagnetic (AFM) order is insulating and therefore suppresses any charge fluctuations, leading to a reduction in  $\chi_c$ . Its residual intensity concentrates around the wavevector  $(\pi, \pi)$ , corresponding to the subleading doublon-hole fluctuations at nearest neighbors [39]. Upon reaching  $\sim 5\%$  doping, the system transforms from the AFM state to stripe fluctuations. The locking of charge and spin stripes results in a prevailing wavevector along the antinodal direction (see the SM [36]) [26, 40].

Beyond 25% hole doping, the stripe fluctuations are gradually supplanted by a checkerboard pattern of charge fluctuation with  $\mathbf{q} = (\pi, \pi)$ . This short-range fluctuation stems from the strong local correlation caused by the repulsive Hubbard  $U$ , which tends to correlate one hole with a neighboring doublon. As the hole doping increases from 25% to 50%, the momentum distribution of charge fluctuations remains qualitatively unchanged,

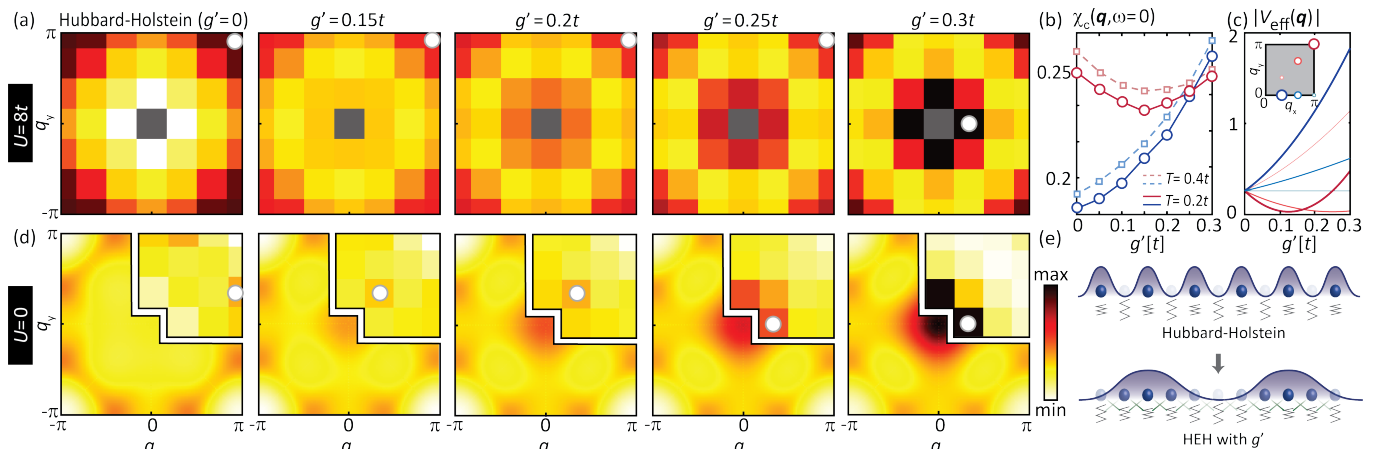


FIG. 3. (a) Charge susceptibility for the quarterly filled HEM model ( $U = 8t$  and  $g = 0.5t$ ) with different  $g'$ 's. (b) Charge susceptibility for  $T = 0.4t$  (dashed curves) and  $T = 0.2t$  (solid curves) as a function of the  $g'$  with  $U = 8t$ . The blue and red curves denote results at the momenta  $(\pi/3, 0)$  and  $(\pi, \pi)$ , respectively. (c) Phonon-mediated effective interaction  $|V_{\text{eff}}(\mathbf{q})|$  for  $\omega = 0$  as a function of  $g'$  at specific momentum points marked in the inset. (d) The  $\chi_c(\mathbf{q})$  obtained by RPA (lower-left) and DQMC (upper-right insets) simulation for the extended-Holstein model with  $U = 0$  and  $T = 0.2t$ . (e) Schematic illustrating that the nonlocal EPC  $g'$  favors longer period charge modulation, while onsite EPC  $g$  favors short period charge modulation.

accompanied by a rapid increase in the overall intensity. This intensification is attributed to unraveled charge carriers from the AFM background. However, this upward trend stops and the susceptibility starts to drop at around quarter filling (50% doping), where a singly-occupied checkerboard pattern develops. Further doping beyond 50% breaks this checkerboard pattern, leading to a drop in intensity.

The evolution of the charge susceptibility, obtained from the Hubbard model, successfully captures the doping dependence of the overall intensity observed in experiments [1]. The maximum at quarter filling reflects the tendency towards a singly-occupied checkerboard pattern, since double occupancy is suppressed by the Hubbard interaction. Therefore, the experimentally observed doping dependence reflects the remnant correlations present in heavily doping cuprates [41–46], not predictable by the Fermi-surface instability. Such an instability is universal in Hubbard models irrespective of specific band structures, as discussed in the SM [36]. It is therefore not surprising that the overdoped CDW is observed in multiple cuprate materials [1, 31].

Nonetheless, the charge susceptibilities of the Hubbard model fail to accurately depict the momentum distribution in experiments [1]. Once the Hubbard model is doped beyond the stripe regime, its charge response consistently manifests dominance at  $\mathbf{q} = (\pi, \pi)$ . Excluding band structure effects (different  $t'$ ) explained in the SM [36], we conclude that the Hubbard model is *insufficient* to address the experimentally observed overdoped CDW. A natural extension of the Hubbard model involves the inclusion of additional interactions. For example, recent studies for 1D cuprate chains have revealed the significance of attractive nonlocal interactions mediated

by phonons [47–52]. Experimental results on underdoped or optimally doped cuprates have further indicated the necessity to include long-range effective interactions, especially attractive ones, to account for the charge order pattern [53, 54]. With these considerations, we introduce EPCs into the Hubbard model and investigate their influence on overdoped CDW. We restrict ourselves to site phonons coupled to electron density ( $n_{i\sigma}$ ) in this paper due to their direct impact on charge density (see SM for a brief discussion about other types of phonons [36]). In the case where the interaction is local, the model corresponds to the Hubbard-Holstein model, with the Hamiltonian:

$$\mathcal{H}_{\text{HH}} = \mathcal{H}_{\text{Hubbard}} + \sum_i \left[ \frac{M}{2} \omega_{\text{ph}}^2 X_i^2 + \frac{P_i^2}{2M} \right] - \sum_{i\sigma} g X_i n_{i\sigma}.$$

Here,  $X_i$  ( $P_i$ ) is the lattice displacement (momentum) at lattice site  $i$ ,  $g$  is the onsite EPC strength,  $M$  is the phonon oscillator mass (set as  $1t^{-1}$ ), and  $\omega_{\text{ph}}$  is the phonon frequency (set as  $1t$ ).

Building upon the Hubbard-model results in Fig. 2, we focus on the momentum distribution of charge susceptibilities at quarter filling ( $n = 0.5$ ) (see the SM [36] for doping dependent results). Due to the numerical complexity associated with phonon degrees of freedom, we employ a  $6 \times 6$  square lattice here, corresponding to the smallest square cluster capable of accommodating the experimentally observed  $(\pi/3, 0)$  momentum. The left-most spectrum in Fig. 3(a) shows  $\chi_c(\mathbf{q}, \omega = 0)$  for the Hubbard-Holstein model with  $g = 0.5t$  meV [55], as determined for 1D cuprate chains (see the SM for different  $g$  values [36]). This result suggests that the presence of the Holstein phonon has a marginal impact on the momentum distribution of  $\chi_c$ , and the susceptibility is still

dominated by the nodal direction near  $(\pi, \pi)$ . The onsite EPC, with a realistic strength, does not qualitatively change the conclusion derived from the Hubbard model.

Thus, we further include nonlocal EPCs. This coupling is found essential in explaining the recently observed attractive interactions in 1D cuprates [47–49]. Due to the distance-dependent decay of electrostatic couplings [48], our primary attention is on the EPC between nearest-neighbor electron density ( $n_{i\sigma}$ ) and lattice displacement ( $X_{i\pm\hat{x}}$  or  $X_{i\pm\hat{y}}$ ), denoted as  $g'$ . This generalized model is referred to as the Hubbard-extended-Holstein (HEH) model. Starting from the quarter-filled Hubbard-Holstein model ( $g' = 0$ ), we gradually increase  $g'$  while fixing  $g = 0.5t$  [see Fig. 3(a)]. In the presence of this nearest-neighbor coupling, a small-momentum charge susceptibility begins to emerge at the zone center. At the same time, the checkerboard charge fluctuations at large momenta maintain their intensities. As  $g'$  increases and exceeds  $\sim 0.25t$ , the small-wavevector  $\chi_c$ , represented by  $\mathbf{q} = (\pi/3, 0)$ , becomes dominant over the  $(\pi, \pi)$  susceptibility [see Fig. 3(b)]. This critical coupling strength is slightly larger than the geometric estimation based on octahedral symmetry, yielding  $g' \sim g/\sqrt{5}$  [48]. Considering the Jahn-Teller effect, the strengths of  $g'$  and  $g$  can be closer in the actual cuprates. Importantly, the intensities at these key wavevectors and their doping dependence are robust against temperature change [see Fig. 3(b)], consistent with the RXS results [1]. Furthermore, while these nonlocal EPCs change the dominant wavevector, they do not affect the doping dependence of the charge susceptibility, which is still maximal near quarter filling (see the SM [36]).

The rise of small-momentum susceptibilities can be elucidated by analyzing the phonon-mediated effective interactions between electrons. The  $g'$  contributes modulation in the EPC of momentum space, i.e.,  $g_{\mathbf{q}} = g + 2g'(\cos q_x + \cos q_y)$ . When  $g'$  shares the same sign of  $g$ , the coupling is predominantly projected to small  $\mathbf{q}$ s. As the phonon-mediated dynamical interaction  $V_{\text{eff}}(\mathbf{q}, \omega) = g_{\mathbf{q}}^2 / M(\omega^2 - \omega_{\text{ph}}^2)$  scales with  $g_{\mathbf{q}}^2$ , this modulation further affects the charge susceptibility at the corresponding momenta [see Figs. 3(b) and (c)]. As a side effect, the momentum dependence of the attractive  $V_{\text{eff}}$  also adjusts the  $(\pi, \pi)$  charges instability. Due to the decrease and eventual negativity of  $g_{\mathbf{q}=(\pi,\pi)}$  with rising  $g'$ , the  $V_{\text{eff}} \propto g_{\mathbf{q}}^2$  displays a nonmonotonic dependence on  $g'$ . Such a non-monotonic relationship is also mirrored in the evolution of  $\chi_c(\mathbf{q} = (\pi, \pi))$ . Alternatively, the impact of nonlocal EPC can be interpreted in the real-space picture. As shown in Fig. 3(e), the presence of  $g'$  clusters electrons around an individual lattice displacement, which turns the short-range doublon-hole fluctuations to form a longer-range charge pattern.

The association of  $V_{\text{eff}}$  and small-momentum charge instabilities suggests an independent origin of these intensities and their coexistence with (large-momentum)

doublon-hole fluctuations induced by  $U$ . These two interactions manifest minimal overlap in momentum space. As a demonstration, we set Hubbard  $U$  to zero in the insets of Fig. 3(d) and find that the DQMC-simulated charge susceptibility intensifies only near the zone center, with little intensity at  $(\pi, \pi)$  compared to that of the HEH model [i.e., Fig. 3(a)]. With EPC of the same strength, these small-momentum susceptibilities are consistent for models with and without  $U$ . The Hubbard  $U$  plays the role of determining the absolute value of charge susceptibility and its doping dependence, without which the maximum cannot be reached at 50% doping.

While the dominant wavevector for charge susceptibility has reached the experimentally observed  $(\pi/3, 0)$  in Fig. 3(a), we avoid over-interpreting the quantitative value of this wavevector, since it is the smallest nonzero wavevector in the  $6 \times 6$  square lattice. As discussed in the SM [36], simulating larger systems (but with a higher temperature) reflects a dominant wavevector closer to  $(0, 0)$ . Moreover, the phonon-mediated  $|V_{\text{eff}}|$  cannot peak at nonzero wavevectors if only positive onsite and nearest-neighbor couplings ( $g$  and  $g'$ ) are considered. Therefore, it is necessary to determine a parameter regime with longer-range couplings (e.g., the next-nearest-neighbor coupling  $g''$ , next-next-nearest-neighbor coupling  $g'''$ , and longer-range coupling  $g''''$ ), where the  $(\pi/3, 0)$  CDW can be more precisely pinned. These terms stem from the electrostatic origin of the site-phonon couplings and contribute to the momentum-space modulation  $g_{\mathbf{q}}$ , which determines the small-momentum charge distributions.

To provide a quick and infinite-resolution estimation of phonon-induced CDW orders, we find that the momentum distribution of  $\chi_c(\mathbf{q})$  can be well estimated by the random phase approximation (RPA), using the  $V_{\text{eff}}(\mathbf{q}, \omega)$  as the vertex. This can be reflected by the comparison of

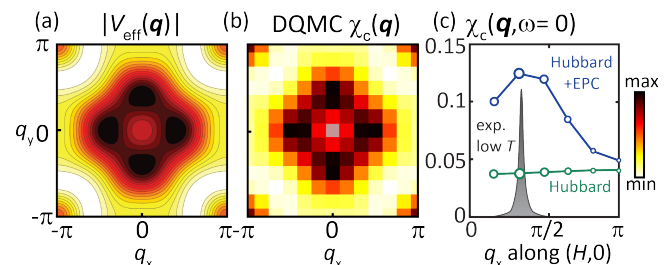


FIG. 4. (a) Effective dynamical interaction  $|V_{\text{eff}}(\mathbf{q}, \omega = 0)|$  mediated by phonons with longer-range interactions ( $g' = 0.2t$ ,  $g'' = -0.1g$ ,  $g''' = g''/\sqrt{2}$ ,  $g'''' = g''/2$ ). (b) DQMC-simulated charge susceptibility  $\chi_c$  for quarter-filled HEM ( $U = 8t$  and  $g = 0.5t$ ) with the interactions in (a), obtained at  $T = 0.5t$ . (c) Comparison of the background-removed scattering results obtained by RXS experiments (shaded gray peak), the antinodal charge susceptibility distribution for the Hubbard model (green), and that for the HEH model (blue).

the major parts (RPA) and insets (DQMC) in Fig. 3(c). This estimation provides a good approximation of the small-momentum instabilities for systems with  $U = 8t$ , since the two interactions determine small- and large-momentum susceptibilities almost independently.

Due to the screening effects at long distances, we slightly release the constraints that EPC decay as  $1/r$ . With the EPC parameter set  $g = 0.5t, g' = 0.2t, g'' = -0.1g, g''' = g''/\sqrt{2}, g'''' = g''/2$  (see the definition of long-range EPC is in the SM [36]), the effective interaction  $|V_{\text{eff}}(\mathbf{q}, \omega = 0)|$  has a peak at  $(\pi/3, 0)$  [see Fig. 4]. Using this parameter set, we simulate  $\chi_c$  by DQMC. As expected, the charge wavevector is precisely pinned at  $(\pi/3, 0)$  for  $12 \times 12$  systems. We use this example to demonstrate the feasibility of inducing a robust charge order consistent with experiments by including long-range EPC. While these couplings are determined by materials' crystal and electronic structures, a slight deviation from this commensurate wavevector may be prevented by domain boundaries in reality. Our simulation ignores the long-range electronic Coulomb repulsion, which contributes an additional  $\sim 1/|\mathbf{q}|^2$  interaction as its bare form. However, the single-band Hubbard model has considered corrections from these Coulomb interactions when projecting from its multi-band prototype [56, 57]. Thus, the effective single-band wavefunction is a composite of copper and oxygen wavefunctions [33], where the in-plane Coulomb interaction has been screened largely by the copper-oxygen covalent bond. Such a screening is more severe in the overdoped regime with a large Fermi surface.

In conclusion, we have explained the emergence of the period-6 CDW in overdoped cuprates. Excluding Fermi-surface instability from Lindhard analyses, the overdoped Hubbard model correctly captures the doping dependence of this CDW, reflecting the remnant correlations even in the overdoped regime. Addressing the constant  $(\pi/3, 0)$  wavevector of this CDW then requires further including EPCs, especially nonlocal EPC, which are determined by geometric relations. The phonon-mediated effective interaction pins the overdoped CDW at  $(\pi/3, 0)$  for a wide range of doping, as seen in RXS experiments. Since the overdoped regime is far from the pseudogap and AFM phases, where spin fluctuations dominate, its phonon-driven nature suggests a subleading interaction in cuprates. This interaction is overwhelmed by the Hubbard  $U$  for underdoped and optimally doped cuprates, as compared in this paper. However, increasing evidence for the contribution of phonons (in addition to strong correlations) to  $d$ -wave superconductivity has been revealed [58–62]. With separable impact from correlations in this overdoped regime, the extracted EPC here is crucial for the theory of unconventional superconductivity.

We thank the experimental inputs from Yingying Peng and insightful discussions from Ilya Esterlis. This work is supported by the Air Force Office of Scientific Research

Young Investigator Program under grant FA9550-23-1-0153. This research used resources of the National Energy Research Scientific Computing Center, a DOE Office of Science User Facility supported by the Office of Science of the U.S. Department of Energy under Contract No. DE-AC02-05CH11231 using NERSC award BES-ERCAP0023810.

---

\* [yao.wang@emory.edu](mailto:yao.wang@emory.edu)

- [1] Q. Li, H.-Y. Huang, T. Ren, E. Weschke, L. Ju, C. Zou, S. Zhang, Q. Qiu, J. Liu, S. Ding, *et al.*, *Prevailing Charge Order in Overdoped Cuprates beyond the Superconducting Dome*, Phys. Rev. Lett. (in press) (2023).
- [2] J. G. Bednorz and K. A. Müller, *Possible High  $T_c$  Superconductivity in the Ba-La-Cu-O System*, Z. Phys. B **64**, 189 (1986).
- [3] E. Dagotto, *Correlated Electrons in High-temperature Superconductors*, Rev. Mod. Phys. **66**, 763 (1994).
- [4] P. A. Lee, N. Nagaosa, and X.-G. Wen, *Doping a Mott Insulator: Physics of High-temperature Superconductivity*, Rev. Mod. Phys. **78**, 17 (2006).
- [5] A. Damascelli, Z. Hussain, and Z.-X. Shen, *Angle-resolved Photoemission Studies of the Cuprate Superconductors*, Rev. Mod. Phys. **75**, 473 (2003).
- [6] D. F. Agterberg, J. S. Davis, S. D. Edkins, E. Fradkin, D. J. Van Harlingen, S. A. Kivelson, P. A. Lee, L. Radzihovsky, J. M. Tranquada, and Y. Wang, *The Physics of Pair-density Waves: Cuprate Superconductors and Beyond*, Annu. Rev. Condens. Matter Phys. **11**, 231 (2020).
- [7] B. Keimer, S. A. Kivelson, M. R. Norman, S. Uchida, and J. Zaanen, *From Quantum Matter to High-temperature Superconductivity in Copper Oxides*, Nature **518**, 179 (2015).
- [8] S. Li, E. Khatami, and S. Johnston, *Competing Phases and Orbital-selective Behaviors in the Two-orbital Hubbard-Holstein Model*, Phys. Rev. B **95**, 121112 (2017).
- [9] T. Shi, E. Demler, and J. I. Cirac, *Variational Study of Fermionic and Bosonic Systems with Non-Gaussian States: Theory and Applications*, Ann. Phys. **390**, 245 (2018).
- [10] I. Esterlis, B. Nosarzewski, E. W. Huang, B. Moritz, T. P. Devereaux, D. J. Scalapino, and S. A. Kivelson, *Breakdown of the Migdal-Eliashberg Theory: A Determinant Quantum Monte Carlo Study*, Phys. Rev. B **97**, 140501 (2018).
- [11] J. S. Davis and D.-H. Lee, *Concepts Relating Magnetic Interactions, Intertwined Electronic Orders, and Strongly Correlated Superconductivity*, Proc. Natl. Acad. Sci. U.S.A. **110**, 17623 (2013).
- [12] S. Peli, S. D. Conte, R. Comin, N. Nembrini, A. Ronchi, P. Abarami, F. Banfi, G. Ferrini, D. Brida, S. Lupi, *et al.*, *Mottness at Finite Doping and Charge Instabilities in Cuprates*, Nat. Phys. **13**, 806 (2017).
- [13] G. Seibold, R. Arpaia, Y. Y. Peng, R. Fumagalli, L. Braicovich, C. Di Castro, M. Grilli, G. C. Ghiringhelli, and S. Caprara, *Strange Metal Behaviour from Charge Density Fluctuations in Cuprates*, Commun. Phys. **4**, 7 (2021).
- [14] S. Lee, E. W. Huang, T. A. Johnson, X. Guo, A. A.

- Husain, M. Mitrano, K. Lu, A. V. Zakrzewski, G. A. de la Peña, Y. Peng, *et al.*, *Generic Character of Charge and Spin Density Waves in Superconducting Cuprates*, Proc. Natl. Acad. Sci. U.S.A. **119**, e2119429119 (2022).
- [15] M. Kang, J. Pelliciani, A. Frano, N. Breznay, E. Schierle, E. Weschke, R. Sutarto, F. He, P. Shafer, E. Arenholz, *et al.*, *Evolution of Charge Order Topology across a Magnetic Phase Transition in Cuprate Superconductors*, Nat. Phys. **15**, 335 (2019).
- [16] M. Rossi, M. Osada, J. Choi, S. Agrestini, D. Jost, Y. Lee, H. Lu, B. Y. Wang, K. Lee, A. Nag, Y.-D. Chuang, C.-T. Kuo, S.-J. Lee, B. Moritz, T. P. Devereaux, Z.-X. Shen, J.-S. Lee, K.-J. Zhou, H. Y. Hwang, and W.-S. Lee, *A Broken Translational Symmetry State in an Infinite-layer Nickelate*, Nat. Phys. **18**, 869 (2022).
- [17] X. Ren, R. Sutarto, Q. Gao, Q. Wang, J. Li, Y. Wang, T. Xiang, J. Hu, F.-C. Zhang, J. Chang, R. Comin, X. J. Zhou, and Z. Zhu, *Symmetry of Charge Order in Infinite-layer Nickelates*, arXiv:2303.02865 (2023).
- [18] C. C. Tam, J. Choi, X. Ding, S. Agrestini, A. Nag, M. Wu, B. Huang, H. Luo, P. Gao, M. García-Fernández, *et al.*, *Charge Density Waves in Infinite-layer NdNiO<sub>2</sub> Nickelates*, Nat. Mater. **21**, 1116 (2022).
- [19] G. Krieger, L. Martinelli, S. Zeng, L. E. Chow, K. Kummer, R. Arpaia, M. Moretti Sala, N. B. Brookes, A. Ariando, N. Viart, M. Salluzzo, G. Ghiringhelli, and D. Preziosi, *Charge and Spin Order Dichotomy in NdNiO<sub>2</sub> Driven by the Capping Layer*, Phys. Rev. Lett. **129**, 027002 (2022).
- [20] J. Tranquada, B. Sternlieb, J. Axe, Y. Nakamura, and S.-i. Uchida, *Evidence for Stripe Correlations of Spins and Holes in Copper Oxide Superconductors*, Nature **375**, 561 (1995).
- [21] R. Comin and A. Damascelli, *Resonant X-ray Scattering Studies of Charge Order in Cuprates*, Annu. Rev. Condens. Matter Phys. **7**, 369 (2016).
- [22] M. Hücker, M. v. Zimmermann, G. D. Gu, Z. J. Xu, J. S. Wen, G. Xu, H. J. Kang, A. Zheludev, and J. M. Tranquada, *Stripe Order in Superconducting La<sub>2-x</sub>Ba<sub>x</sub>CuO<sub>4</sub> (0.095 ≤ x ≤ 0.155)*, Phys. Rev. B **83**, 104506 (2011).
- [23] E. H. da Silva Neto, P. Aynajian, A. Frano, R. Comin, E. Schierle, E. Weschke, A. Gyenis, J. Wen, J. Schneeloch, Z. Xu, *et al.*, *Ubiquitous Interplay between Charge Ordering and High-temperature Superconductivity in Cuprates*, Science **343**, 393 (2014).
- [24] E. Fradkin, S. A. Kivelson, and J. M. Tranquada, *Colloquium: Theory of Intertwined Orders in High Temperature Superconductors*, Rev. Mod. Phys. **87**, 457 (2015).
- [25] B. Loret, N. Auvray, Y. Gallais, M. Cazayous, A. Forget, D. Colson, M.-H. Julien, I. Paul, M. Civelli, and A. Sacuto, *Intimate Link between Charge Density Wave, Pseudogap and Superconducting Energy Scales in Cuprates*, Nat. Phys. **15**, 771 (2019).
- [26] E. W. Huang, C. B. Mendl, H.-C. Jiang, B. Moritz, and T. P. Devereaux, *Stripe Order from the Perspective of the Hubbard Model*, npj Quantum Mater. **3**, 1 (2018).
- [27] B.-X. Zheng, C.-M. Chung, P. Corboz, G. Ehlers, M.-P. Qin, R. M. Noack, H. Shi, S. R. White, S. Zhang, and G. K.-L. Chan, *Stripe Order in the Underdoped Region of the Two-dimensional Hubbard Model*, Science **358**, 1155 (2017).
- [28] S. Jiang, D. J. Scalapino, and S. R. White, *Ground-state Phase Diagram of the  $t-t'-J$  Model*, Proc. Natl. Acad. Sci. U.S.A. **118**, e2109978118 (2021).
- [29] H.-C. Jiang and T. P. Devereaux, *Superconductivity in the Doped Hubbard Model and Its Interplay with Next-nearest Hopping  $t'$* , Science **365**, 1424 (2019).
- [30] H. Xu, C.-M. Chung, M. Qin, U. Schollwöck, S. R. White, and S. Zhang, *Coexistence of Superconductivity with Partially Filled Stripes in the Hubbard Model*, arXiv:2303.08376 (2023).
- [31] Y. Peng, R. Fumagalli, Y. Ding, M. Minola, S. Caprara, D. Betto, M. Bluschke, G. De Luca, K. Kummer, E. Lefrançois, *et al.*, *Re-entrant Charge Order in Overdoped (Bi,Pb)<sub>2.12</sub>Sr<sub>1.88</sub>CuO<sub>6+δ</sub> Outside the Pseudogap Regime*, Nat. Mater. **17**, 697 (2018).
- [32] J. Hubbard, *Electron Correlations in Narrow Energy Bands*, Proc. Math. Phys. Eng. Sci. **276**, 238 (1963).
- [33] F. C. Zhang and T. M. Rice, *Effective Hamiltonian for the Superconducting Cu Oxides*, Phys. Rev. B **37**, 3759 (1988).
- [34] E. Pavarini, I. Dasgupta, T. Saha-Dasgupta, O. Jepsen, and O. K. Andersen, *Band-structure Trend in Hole-doped Cuprates and Correlation with  $T_c$  Max*, Phys. Rev. Lett. **87**, 047003 (2001).
- [35] T. Yoshida, X. J. Zhou, K. Tanaka, W. L. Yang, Z. Hussain, Z.-X. Shen, A. Fujimori, S. Sahrakorpi, M. Lindroos, R. S. Markiewicz, A. Bansil, S. Komiyama, Y. Ando, H. Eisaki, T. Kakeshita, and S. Uchida, *Systematic doping evolution of the underlying Fermi surface of La<sub>2-x</sub>Sr<sub>x</sub>CuO<sub>4</sub>*, Phys. Rev. B **74**, 224510 (2006).
- [36] See the Supplementary Materials for discussions regarding the impact of band structures on  $\chi_c$ , a low-temperature Hubbard model simulation, a brief analysis of non-Holstein phonons, and the size and interaction dependence of the Hubbard-Holstein and HEH-model results.
- [37] R. Blankenbecler, D. Scalapino, and R. Sugar, *Monte Carlo Calculations of Coupled Boson-fermion systems. I*, Phys. Rev. D **24**, 2278 (1981).
- [38] S. R. White, D. J. Scalapino, R. L. Sugar, E. Y. Loh, J. E. Gubernatis, and R. T. Scalettar, *Numerical Study of the Two-Dimensional Hubbard Model*, Phys. Rev. B **40**, 506 (1989).
- [39] E. A. Nowadnick, S. Johnston, B. Moritz, R. T. Scalettar, and T. P. Devereaux, *Competition Between Antiferromagnetic and Charge-density-wave Order in the Half-filled Hubbard-Holstein Model*, Phys. Rev. Lett. **109**, 246404 (2012).
- [40] E. W. Huang, C. B. Mendl, S. Liu, S. Johnston, H.-C. Jiang, B. Moritz, and T. P. Devereaux, *Numerical Evidence of Fluctuating Stripes in the Normal State of High- $T_c$  Cuprate Superconductors*, Science **358**, 1161 (2017).
- [41] M. Dean, G. Dellea, R. S. Springell, F. Yakhov-Harris, K. Kummer, N. Brookes, X. Liu, Y. Sun, J. Strle, T. Schmitt, *et al.*, *Persistence of Magnetic Excitations in La<sub>2-x</sub>Sr<sub>x</sub>CuO<sub>4</sub> from the Undoped Insulator to the Heavily Overdoped Non-superconducting Metal*, Nat. Mater. **12**, 1019 (2013).
- [42] C. Jia, E. Nowadnick, K. Wohlfeld, Y. Kung, C.-C. Chen, S. Johnston, T. Tohyama, B. Moritz, and T. Devereaux, *Persistent Spin Excitations in Doped Antiferromagnets Revealed by Resonant Inelastic Light Scattering*, Nat. Commun. **5**, 3314 (2014).
- [43] J. Graf, G.-H. Gweon, K. McElroy, S. Y. Zhou, C. Jozwiak, E. Rotenberg, A. Bill, T. Sasagawa, H. Eisaki, S. Uchida, H. Takagi, D.-H. Lee, and A. Lanzara, *Universal High Energy Anomaly in the Angle-*

- Resolved Photoemission Spectra of High Temperature Superconductors: Possible Evidence of Spinon and Holon Branches*, Phys. Rev. Lett. **98**, 067004 (2007).
- [44] M. Le Tacon, G. Ghiringhelli, J. Chaloupka, M. M. Sala, V. Hinkov, M. Haverkort, M. Minola, M. Bakr, K. Zhou, S. Blanco-Canosa, *et al.*, *Intense Paramagnon Excitations in a Large Family of High-temperature Superconductors*, Nat. Phys. **7**, 725 (2011).
- [45] W. Lee, J. Lee, E. Nowadnick, S. Gerber, W. Tabis, S. Huang, V. Strocov, E. Motoyama, G. Yu, B. Moritz, *et al.*, *Asymmetry of Collective Excitations in Electron- and Hole-doped Cuprate Superconductors*, Nat. Phys. **10**, 883 (2014).
- [46] K. Ishii, M. Fujita, T. Sasaki, M. Minola, G. Dellea, C. Mazzoli, K. Kummer, G. Ghiringhelli, L. Braicovich, T. Tohyama, *et al.*, *High-energy Spin and Charge Excitations in Electron-doped Copper Oxide Superconductors*, Nat. Commun. **5**, 3714 (2014).
- [47] Z. Chen, Y. Wang, S. N. Rebec, T. Jia, M. Hashimoto, D. Lu, B. Moritz, R. G. Moore, T. P. Devereaux, and Z.-X. Shen, *Anomalously Strong Near-neighbor Attraction in Doped 1D Cuprate Chains*, Science **373**, 1235 (2021).
- [48] Y. Wang, Z. Chen, T. Shi, B. Moritz, Z.-X. Shen, and T. P. Devereaux, *Phonon-mediated Long-range Attractive Interaction in One-dimensional Cuprates*, Phys. Rev. Lett. **127**, 197003 (2021).
- [49] T. Tang, B. Moritz, C. Peng, Z.-X. Shen, and T. P. Devereaux, *Traces of Electron-phonon Coupling in One-dimensional Cuprates*, Nat. Commun. **14**, 3129 (2023).
- [50] A. E. Feiguin, C. Helman, and A. A. Aligia, *Effective One-band Models For the One-dimensional Cuprate  $Ba_{2-x}Sr_xCuO_{3+\delta}$* , Phys. Rev. B **108**, 075125 (2023).
- [51] H.-X. Wang, Y.-M. Wu, Y.-F. Jiang, and H. Yao, *Spectral Properties of 1D Extended Hubbard Model from Bosonization and Time-Dependent Variational Principle: Applications to 1D Cuprate*, arXiv:2211.02031 (2022).
- [52] D. Banerjee, J. Thomas, A. Nocera, and S. Johnston, *Ground-state and Spectral Properties of the Doped One-dimensional Optical Hubbard-Su-Schrieffer-Heeger Model*, Phys. Rev. B **107**, 235113 (2023).
- [53] F. Boschini, M. Minola, R. Sutarto, E. Schierle, M. Bluschke, S. Das, Y. Yang, M. Michiardi, Y. Shao, X. Feng, *et al.*, *Dynamic Electron Correlations with Charge Order Wavelength along All Directions in the Copper Oxide Plane*, Nat. Commun. **12**, 1 (2021).
- [54] K. Scott, E. Kisiel, T. J. Boyle, R. Basak, G. Jargot, S. Das, S. Agrestini, M. Garcia-Fernandez, J. Choi, J. Pelliciani, *et al.*, *Low-energy Quasi-circular Electron Correlations with Charge Order Wavelength in  $Bi_2Sr_2CaCu_2O_{8+\delta}$* , Sci. Adv. **9**, eadg3710 (2023).
- [55] Due to the variation of the hopping  $t$  obtained by different fitting approaches [34, 35], the absolute value of  $g$  is between 130-210 meV, falling in the range determined by 1D cuprates [48].
- [56] M. S. Hybertsen, E. B. Stechel, M. Schluter, and D. R. Jennison, *Renormalization from Density-functional Theory to Strong-coupling Models for Electronic States in Cu-O Materials*, Phys. Rev. B **41**, 11068 (1990).
- [57] P. Hansmann, N. Parragh, A. Toschi, G. Sangiovanni, and K. Held, *Importance of  $d - p$  Coulomb Interaction for High  $T_c$  Cuprates and Other Oxides*, New J. Phys. **16**, 033009 (2014).
- [58] Y. He, M. Hashimoto, D. Song, S.-D. Chen, J. He, I. Vishik, B. Moritz, D.-H. Lee, N. Nagaosa, J. Zaanen, *et al.*, *Rapid Change of Superconductivity and Electron-phonon Coupling through Critical Doping in Bi-2212*, Science **362**, 62 (2018).
- [59] M. Jiang, *Enhancing  $d$ -wave Superconductivity with Nearest-neighbor Attraction in the Extended Hubbard Model*, Phys. Rev. B **105**, 024510 (2022).
- [60] C. Peng, Y. Wang, J. Wen, Y. S. Lee, T. P. Devereaux, and H.-C. Jiang, *Enhanced Superconductivity by Near-neighbor Attraction in the Doped Extended Hubbard Model*, Phys. Rev. B **107**, L201102 (2023).
- [61] H.-X. Wang, Y.-F. Jiang, and H. Yao, *Robust  $d$ -wave Superconductivity from the Su-Schrieffer-Heeger-Hubbard Model: Possible Route to High-temperature Superconductivity*, arXiv:2211.09143 (2022).
- [62] X. Cai, Z.-X. Li, and H. Yao, *High-temperature Superconductivity Induced by the Su-Schrieffer-Heeger Electron-phonon Coupling*, arXiv:2308.06222 (2023).